Pergamon

Journal of Structural Geology, Vol. 18, Nos 2/3, pp. 281 to 293, 1996

0191-8141/96 $15.00 + 0.00

0191-8141(95)00132-8

Are fault growth and linkage models consistent with power-law distributions of fault lengths?

TRENTON T. CLADOUHOS

Department of Geological Sciences, Box 351310, University of Washington, Seattle, WA 98195, U.S.A.

and

RANDALL MARRETT

Department of Geological Sciences, University of Texas at Austin, Austin, TX 78712, U.S.A.

(*Received* 3 *January* 1995; *accepted in revised form* 17 *October* 1995)

Abstract—It has recently been recognized that fault lengths (L) in natural populations follow power-law scaling. Such power-law scaling is observed in a wide range of tectonic settings in regions that have experienced differing amounts of total strain, and exhibit faults over a very large range of dimensions. In this paper we explore possible constraints on fault growth and linkage required to maintain power-law length scaling during progressive deformation. We first consider a fault growth model in which individual faults in a population grow by an amount $\Delta L \propto L^F$ during slip increments (earthquakes), which have a recurrence interval $\tau \propto L^E$. If an initial power-law length distribution is assumed for the population, it is found that the growth model exponents must be related by $F - E = 1$ in order to continually maintain the same scaling. If the requirement of constant moment release rate through time is also imposed, this implies that for large faults $E = 2$, which leads to a loss of power-law scaling with increasing strain, unless $F = 3$. Current mechanical models for growth of single faults by tip propagation propose $E \geq 1$ and $F = 1$. Thus single-fault models are not consistent with observed power-law scaling. In a second model, fault lengths increase by growth specified by the first model, unless a nearby fault is encountered, in which case the two faults link. With this model, it is possible to produce a power-law distribution from a fault or flaw population that initially does not have a power-law distribution. Once a power-law distribution is developed, fault linkage causes the power-law exponent (C) to decrease as fault strain increases.

INTRODUCTION

Several recent field studies have demonstrated that fault populations have a power-law length distribution (Shaw & Gartner 1986, Gudmundsson 1987, Villemin & Sunwoo 1987, Main *et al.* 1990, Scholtz & Cowie 1990, Scholz *et al.* 1990, Davy 1993). In a fault population with a power-law length distribution, the number of faults (N) of length $\geq L$ is

$$N_{\geq L} = \left(\frac{L}{L_{\max}}\right)^{-C}, \quad (1)$$

where $L_{\max}$ is the length of the longest fault. Fault length data are usually evaluated on a log–log graph, in which case fault length (L) versus fault rank (N) data falls on a line with a slope of $-C$. Previously published data suggest that C varies between 1.1 and 1.6 (Villemin & Sunwoo 1987, Main *et al.* 1990, Scholz & Cowie 1990). The data presented in Fig. 1 were collected from existing fault maps (five published geologic maps and three unpublished Amoco Production Company maps from the Gulf of Mexico), and suggest an even larger range of C (0.67–2.07).

Fault length data are well described by power-law distributions; however, because fault mapping is not usually specifically performed for fault length analysis, the fault length data may be biased. At least two systematic problems related to the mapping of fault traces may affect this data. In an incompletely exposed region, it is often difficult to interpret whether or not two fault traces separated by a covered area represent the same fault. Failure to recognize the connectivity of distinct fault trace exposures will result in estimates of C that are too high. Even a fault trace map of a completely exposed region may be systematically biased if the map represents the loci of displacements greater than some threshold value. If the displacement profiles of faults are scale invariant, then larger portions of small faults will be unmapped compared to large faults. Consequently, the apparent C will be too low. In summary, while it is probable that equation (1) correctly describes fault length populations, the actual value and range of C, both here and elsewhere in the literature, is not as well determined.

Total fault displacement also scales as a power-law of length (Walsh & Watterson 1988, Marrett & Allmendinger 1991, Cowie & Scholz 1992b, Gillespie *et al.* 1992, Dawers *et al.* 1993):

$$D \propto L^n. \quad (2)$$

Again, on a log–log graph, fault length (L) vs total fault displacement (D) falls on a line with a slope of n. The data presented in Walsh & Watterson (1988) and Mar-

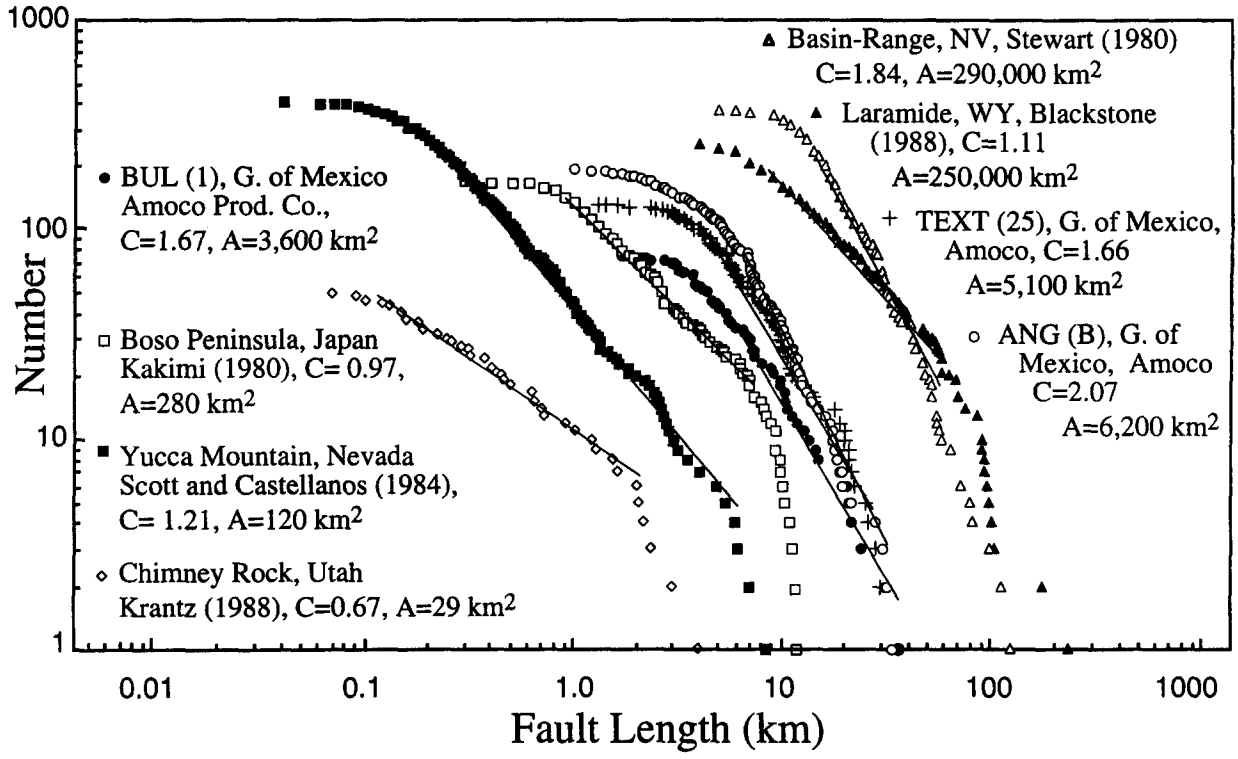

Fig. 1. Eight fault length data sets derived from the maps published in the references given on the figure. Thin lines show the portions of the curves which fit lines with slopes of C. Because these data were collected from two-dimensional samples of three-dimensional volumes, equation (1) and the data in Fig. 1 describe two-dimensional fault populations. The actual (three-dimensional) power-law exponent for small faults is $C + 1$ (Marrett & Allmendinger 1991). Also shown are the areas (A) in square kilometers of the maps from which the data were collected.

rett & Allmendinger (1991) fit equation (2) with $n \approx 1.5$. From theoretical mechanical arguments and smaller data sets Cowie & Scholz (1992a,b) and Dawers *et al.* (1993) suggest that $n = 1.0$ is more likely.

The relationships in equations (1) and (2) are important because they can be used to quantify fault-strain (Jamison 1989) within a region (e.g. Scholz & Cowie 1990, Marrett & Allmendinger 1990, 1991). Uncertainty regarding the values of the exponents (C and n) currently limits our ability to derive strain elements from fault populations.

Most fault growth models (e.g. Cowie & Scholz 1992c) examine the growth of an individual fault from a mechanical or seismological standpoint. Due to the short observational scale of seismological and paleoseismological studies, these models are impossible to test directly. The entire growth history of an individual fault cannot be examined. Rather, geologists are forced to look at fault populations that include a full range of sizes; therefore equations (1) and (2), which, though empirical, characterize real fault populations, may provide the best constraints on fault growth.

Two different models are presented in this paper. The first model considers growth of individual faults by tip propagation during slip events (earthquakes) in which each growth increment depends, in a simple and direct way, on the size of the earthquake and the length of the fault. We explore how fault growth by this mechanism affects the development of a fault population that initially has a power-law distribution of lengths. The second model incorporates fault linkage which depends upon spatial properties of the fault population as well as individual fault length. The second model addresses the establishment of a power-law distribution in an undeformed region, and the evolution of that power-law distribution once established. In the following sections, the *fault growth model* refers to the process of fault lengthening by tip rupture (i.e. creating new fault length), whereas the *fault linkage model* refers to fault lengthening by coalesence with other faults (i.e. long faults formed by cannibalizing smaller faults).

FAULT GROWTH MODEL

In this section, an initial power-law distribution is assumed. Then, assuming a constant number of faults (no fault birth or death), equations are developed to describe a fault growth model which simulates slip events (earthquakes) that will maintain the population's power-law exponent. Although the following population fault growth model may borrow concepts and equations from single-fault growth models, the final goal of maintaining the power-law exponent may lead to different conclusions between population and single-fault models.

Growth increment and recurrence

Most single-fault growth models (Cowie & Scholz 1992a,c, Gillespie *et al.* 1992, Walsh & Watterson 1992)

use the hypothetical convenience of the 'equivalent' earthquake which ruptures the entire length of a fault. Because real earthquakes seldom rupture the entire fault, the equivalent earthquake may represent a composite of many earthquakes, which in combination slip the entire fault surface. In this case, the equivalent earthquake represents a complete seismic cycle of a fault. Because of the difference between real and equivalent earthquakes, a fault growth model may not explicitly satisfy a power-law distribution of earthquakes (Gutenburg & Richter 1954, Aki 1981, Turcotte 1992) although that issue is explored by Cladouhos (1993).

An equivalent earthquake causes a fault to lengthen by an amount ΔL:

$$L_F = L_i + \Delta L, \tag{3}$$

where L_i is the fault length before the event and L_f is the fault length after the event. To model the growth of faults within a population, two major assumptions about the equivalent earthquakes must be made. Firstly, a model for the growth increment, ΔL, must be assumed. In this paper a general growth model is explored:

$$\Delta L = \lambda L_i^F, \tag{4}$$

where λ and F are constants.

The value of F in equation (4) can be analytically determined by adopting a specific fault growth model. For example, Marrett & Allmendinger (1991) and Gillespie *et al.* (1992) developed a fault growth model based on an arithmetic series, in which the difference between successive slips depends linearly upon the total number of slip events that have occurred on the fault. In that case, ΔL will depend upon the square root of fault length ($F = 0.5$), and total fault displacement is scaled by $n = 1.5$. Gillespie *et al.* (1992) argue that because the stress intensity factor at the tip of a fault in an elastic medium is also dependent upon the square root of fault length, their model has a mechanical basis. Meanwhile, Cowie & Scholz (1992a) consider the inelastic deformation at the fault tip (the process zone) to control fault growth. Their model, which is based upon a cohesion zone model for the crack tip (Dugdale 1960), gives a linear relation between ΔL, L, and D ($F = 1, n = 1$). It is not the purpose of this paper to choose between these competing single-fault models, but to test both for consistency with power-law fault length distribution.

The second assumption involves the recurrence interval (τ) of the equivalent earthquake. Again, the most general case is explored and the recurrence interval is written as:

$$\tau = \tau_\kappa L^E, \tag{5}$$

where τ_k and E are constants. Note that equation (5) implies the following relationship between slip rate ($\dot{u}$) and fault length: $\dot{u} \sim L^{1-E}$.

Equations (4) and (5) define the fault growth model due to slip events. Note that the fault growth exponents F and E are unrelated to C, the exponent that describes the power-law size distribution of the fault population (equation 1).

By assuming that the recurrence interval of an individual equivalent earthquake (10^2–10^3 a) is small compared to the total age of a fault (>10^6 a) (i.e. Cowie & Scholz 1992c), and writing a differential equation we can solve for fault growth as a function of time:

$$\frac{dL}{dt} = \frac{\Delta L}{\tau} = \frac{\lambda L^F}{\tau_k L^E} = \frac{\lambda}{\tau_k} L^{F-E}. \tag{6}$$

Before integration, the form of equation (6) can be further specified by assuming that the power-law distribution described by equation (1) is maintained as the individual faults in a population grow. Because the rank (N) of a fault will not change as it grows, the ratio between any two fault lengths will remain constant. If the superscripts in the equation below represent the A^{th} and B^{th} longest faults, equation (1) can be used to write:

$$\left(\frac{L_A(t)}{L_B(t)}\right)^{-C} = \left(\frac{L_A(t+\Delta t)}{L_B(t+\Delta t)}\right)^{-C} \tag{7}$$

where Δt is an increment (not necessarily infinitesimal) of time. Using equation (6), equation (7) can be rewritten as

$$\frac{L_A}{L_B} = \frac{L_A + \dfrac{\Delta L}{\tau}\Delta t}{L_B + \dfrac{\Delta L}{\tau}\Delta t} = \frac{L_A + \dfrac{\lambda}{\tau_k} L_A^{F-E}\Delta t}{L_B + \dfrac{\lambda}{\tau_k} L_B^{F-E}\Delta t}. \tag{8}$$

The equality in the above equation is insured only if

$$F - E = 1. \tag{9}$$

Thus, a relationship between the growth increment and the recurrence interval has been established. The results of simple numerical modeling shown in Fig. 2 confirm that the relation in equation (9) is necessary to insure that a power-law length distribution is maintained for a population of growing faults in which there are no fault births or deaths. As shown in Fig. 2, other relationships between F and E produce populations that cannot be fit by a line in log–log space.

Integration of equation (6) for the special case of $F - E = 1$ gives:

$$L(t) = L_0 \exp\left(\frac{\lambda t}{\tau_k}\right) \tag{10}$$

Given the assumptions of the population fault growth model—no fault deaths or births, and constant power-law length distribution—fault growth must be exponential with time. A further constraint on the fault growth model can be made by requiring that the moment release rate, which is a measure of strain rate, remain constant. The seismic moment (M_0) of an earthquake occurring on a fault of length L is:

$$M_0 = \mu\alpha L^2 W, \quad \text{for large faults, and} \tag{11a}$$

$$M_0 = \mu\alpha L^3(\pi/4), \quad \text{for small faults} \tag{11b}$$

where μ is the shear modulus, α a constant that relates earthquake slip and fault length ($u = \alpha L$, Kanamori & Anderson 1975) and W is the dimension of the fault

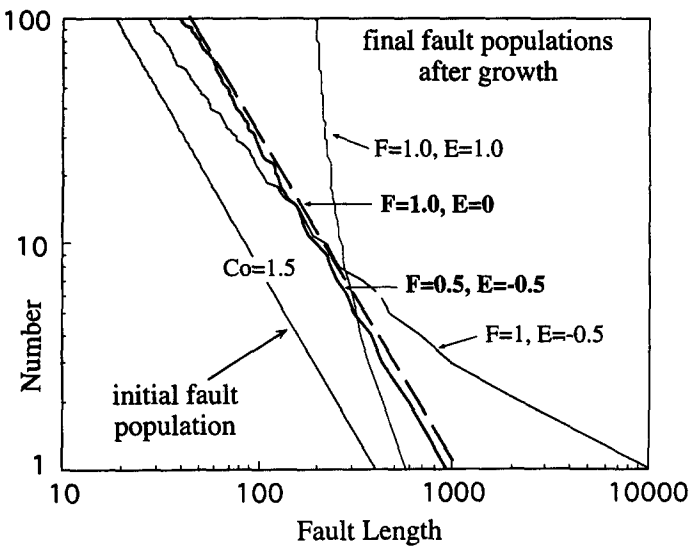

Fig. 2. Results of four runs of a simple numerical model to simulate a population of growing faults. The critical assumption of the numerical modeling is that all faults in a population are actively growing; i.e. faults do not die. The initial (assumed) population (far left line) contains 100 faults, the longest fault is 400 units long, and the power law exponent is $C_0 = 1.5$. The choice of C_0 is arbitrary; the results do not depend on the value of C_0. The other four curves represent possible fault populations after on the order of one thousand equivalent earthquakes on each fault. The growth increment for each fault was specified by equation (4), and the value of F shown on the figure. Recurrence interval for each fault was specified by equation (5) and the value of E specified on the figure. These four runs and numerous others (Cladouhos 1993) confirm the assertion in the text that $F - E = 1$ (bold lines) is necessary to maintain a power-law distribution.

plane perpendicular to the slip direction (plate thickness). For a steady-state deformation, the total moment release rate for a fault population should remain constant. This requires that each fault in the population must have a constant moment release rate ($\dot{M}_0$) also. The seismic moment and the moment release rate for each fault are related by its recurrence interval:

$$\tau = \frac{M_0}{\dot{M}_0}. \tag{12}$$

Substituting equation (11) into equation (12), and recasting in the form of equation (5) gives

$$E = 2 \text{ and } \tau_k = \frac{\mu \alpha W}{\dot{M}_0} \quad \text{for large faults and} \tag{13a}$$

$$E = 3 \text{ and } \tau_k = \frac{\mu \alpha \pi}{4\dot{M}_0} \quad \text{for small faults.} \tag{13b}$$

The relation shown by equation (9) uniquely specifies F as well. If a constant moment release rate is required, $F = 3$ for large faults and $F = 4$ for small faults.

DISCUSSION OF FAULT GROWTH MODEL

The model developed here is an important departure from single-fault growth models. For example, in the Cowie & Scholz (1992c) model, the exponents for a fault that grows under constant slip rate are $F = 1$ and $E = 1$. If constant moment release rate is required, then $F = 1$ and $E = 2$ for large faults. However, as shown by the curve for $F = E = 1$ on Fig. 2, that model is not consistent with a power-law distribution of fault lengths. This is because the relatively long recurrence intervals for long faults limits their growth compared to smaller faults. After a time increment the fault population curve becomes non-linear on the log–log plot, and the overall slope steepens.

On the other hand, a constant moment release rate population fault growth model implies growth increment exponents ($F = 3$ or $F = 4$) and recurrence interval exponents ($E = 2$ or $E = 3$) which are much higher than any single-fault growth model has suggested. Thus, current mechanical models for the growth of individual faults may not be consistent with power-law distributions of fault lengths. In other words, some other mechanism of fault lengthening must be operating in addition to incremental tip growth during repeated slip events.

The apparent discrepancy between single-fault growth models and population fault growth model presented here might be resolved by *rejecting* one or more of the assumptions used to formulate the fault population model. First, some faults in the population could cease to be active during deformation (i.e. faults could die) or new faults could nucleate during deformation (i.e. fault birth could occur). Second, the power-law scaling exponent C need not remain constant throughout deformation. If C is allowed to increase with accumulating fault strain, then $F - E < 1$ is a feasible solution; however, fault length data will no longer strictly fit a line in log–log space (i.e. Fig. 2). Third, if faults do not grow under steady state deformation conditions (constant moment release rate), the unreasonable values of the exponents ($F = 3$, $E = 2$ for large faults and $F = 4$, $E = 3$ for small faults) need not be enforced. If the moment release rate is allowed to increase, then lower values of F and E can be chosen (i.e. $F = 1$, $E = 0$). Fourth, individual fault growth cannot be specified by scale invariant equations (equations (4) and (5)) that do not depend upon a fault population's spatial properties. For example, other processes which depend upon the spatial distribution of the faults, such as fault linkage, may be responsible for maintaining the power-law distribution.

FAULT LINKAGE MODEL

Background

In the previous section, initial power-law distributions were assumed, and the evolution of a model population of growing faults examined. In this section, to explore how power-law distributions are initially developed, an initial distribution that is not power-law distributed is assumed. This is based on a fundamental mechanical concept of rock mechanics, Griffith cracks, which may introduce a length scale. This theory, first proposed by Griffith (1920, 1924) holds that ubiquitous microfrac-

tures cause rocks to be much weaker than their theoretical strength. More recently, it has been accepted that macroscopic rock fracture occurs due to the coalescence of Griffith cracks (i.e. Suppe 1985, p.159). Like macrofractures and faults, microfractures (1–100 microns) may be power-law distributed (Wong *et al.* 1989). One purpose of this section is to show that in some instances, a power-law length distribution can result from a population that is not initially power-law distributed. For the model constructed below, Griffith cracks (flaws) are assumed to have a unimodal distribution. This is consistent with stress tests on Westerly granite, which showed that biotite grains, the lengths of which are normally distributed, were often the locus of microcracking (Tapponier & Brace 1976). This finding is also used to justify the assumption that flaws are pre-existing weaknesses within a rock which may be activated by deformation, but are not created by the deformation.

To develop a power-law distribution of faults from a unimodal length distribution of flaws, an uneven growth process is necessary. We hypothesize that fault linkage provides the mechanism for faults to grow unevenly, and thus causes fault populations to develop power-law length distributions. In this section, a simple model that starts with a unimodal distribution of flaws is developed. In each slip event, the length of a fault increases by one of two mechanisms: if another fault tip is nearby the two faults link, forming a much larger fault (Fig. 3); otherwise, the fault propagates as discussed in the previous section on Fault Growth Models. Because explicit numerical modeling of a mechanical system containing hundreds of faults would be extremely complex, we use simple geometrical rules, based on mechanical concepts, to model the fault interactions.

Fault linkage has been well-documented in the field (Segall & Pollard 1983, Martel *et al.* 1988, Childs *et al.* 1990, Martel 1990, Peacock 1991, Peacock & Sanderson 1991). Martel *et al.* (1988) and Martel (1990) describe a three-stage evolution of outcrop-scale faults within Sierra Nevada granites; the faulting begins with jointing, then progresses to slip on small faults, and evolves by fault linkage to form larger fault zones. We consider the fault linkage process to be scale invariant; faults of all sizes link to form larger faults.

Pollard & Segall (1987) give a formula in polar coordinates (r, θ) for the stress near the tip of a fault in elastic material:

$$\sigma_{ij} \cong \Delta\sigma_{II}\left(\frac{L}{2r}\right) f_{ij}(\theta), \quad (\text{for } r < L), \tag{14}$$

where $\Delta\sigma_{II}$ is the driving shear stress on a mode II crack, and $f_{ij}(\theta)$ a trigonometric term that depends on the stress component. Note that in equation (14) the elastic stress is a linear function of fault length (L).

The linkage model

The purpose of the linkage model developed in this section is to investigate the effect of linkage on length distributions of fault populations. The model's purpose is not to accurately model the mechanics of fault linkage. We take a simplistic approach to linkage and assume that the elastic stress field produced by a fault, which according to equation (14) depends upon fault length, can influence the behavior of nearby faults. We assume that when two tips are close enough to elastically 'feel' each other, the elastic stresses are increased so that the faults 'attract' each other.

A simple criterion is used to determine whether two fault tips are close enough to link. For the purpose of the model, a circular region of radius r_{max} located at the tip of the fault is defined (Fig. 3). If another fault tip is located within that region, the faults will link (Fig. 3a). If another fault is not located within that region, the fault will propagate by the mode discussed in the previous

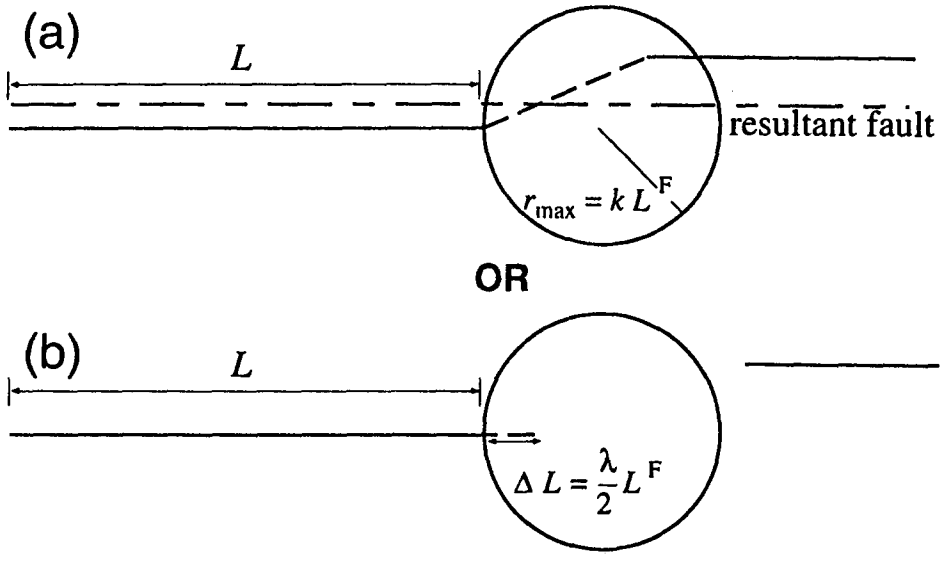

Fig. 3. Schematic description of the fault linkage model. (a) If another fault tip occurs within a circle of radius r_{max}, the two faults will link. In order to simplify the model, the resulting larger fault, shown by the long dash–short dash line, is straightened. (b) If no tip occurs within the radius, the fault will propagate forward a distance of ΔL.

section (Fig. 3b). In the fault growth model of the previous section, fault growth due to a single event depended upon a variable power (F) of fault length. We propose that any criteria for linkage should be dependent upon the same variable exponent:

$$r_{max} = kL^F. \quad (15)$$

where k is an adjustable parameter which controls the radius of the search circle shown in Fig. 3.

Of course, real fault linkage is much more complicated. Firstly, the shape of the elastic field around a fault tip is not circular as portrayed in Fig. 3 (Pollard & Segall 1987); however, for the purpose of examining a hypothetical fault population with random locations, the area enclosed by a specific elastic stress contour (not the shape of the contour) should be the controlling factor. Secondly, if a fault tip grows into the compressional field of another fault, the fault tip may be 'repelled'. This possibility is not modeled. Lastly, in this model, faults only link at the tips; real linkage may occur after the fault tips have overlapped (Peacock 1991).

The actual linkage model is a 650 × 650 grid initially populated with 500 five-unit-long flaws (Griffith cracks) with random locations (Fig. 4a—top). To limit the effect of the lateral boundaries, a periodic boundary condition is used: a fault that grows and hits the right edge reemerges at the left edge and vice versa. During each step of model time a flaw may grow by either tip propagation (equations (4) and (5)) or by linkage (Fig. 3a). For the purpose of this model, a fault is formed when two flaws link. The necessity for this distinction between flaws and faults is shown in Fig. 5(a). All flaws initially have the same length, as is shown by the vertical line labeled $t0$ in Fig. 5(a). After each step of model time, all unlinked flaws will have grown by the same amount because the flaw growth rate depends on flaw length. Thus, unlinked flaws will maintain a unimodal distribution (i.e. $C = \infty$) as shown by the vertical lines in Fig. 5(a). At each step of model time, some flaws may coalesce with other flaws to form much longer faults. Due to continued linkage, the faults grow much faster than the flaws and form a power-law distribution with C between 6.7 and 0.9. If flaws and faults are not separated and a linear fit attempted on both flaws and faults, the value of C would always be large and dominated by the flaws.

The values of the growth increment and recurrence interval exponents (F and E) will affect the size distribution that results from a run of the fault linkage model. In order to isolate the effect of linkage on the power law exponent C, a population fault growth model that does not change the value of C (i.e. $F = 1$, $E = 0$) was chosen for most of the model runs. The model was also run with $F = E = 1$ (Cowie & Scholz 1992c), and those results are shown along with the more numerous results with $F - E = 1$.

As noted earlier, using $F = 1$ and $E = 0$ as growth exponents implies an increasing moment release rate, which is not appropriate for a steady-state deformation. However, this choice of exponents may be appropriate for the early stages of a deformation episode during which time the power-law distribution is developed. With $E = 0$, the recurrence interval does not depend upon fault length, and every fault in the population has

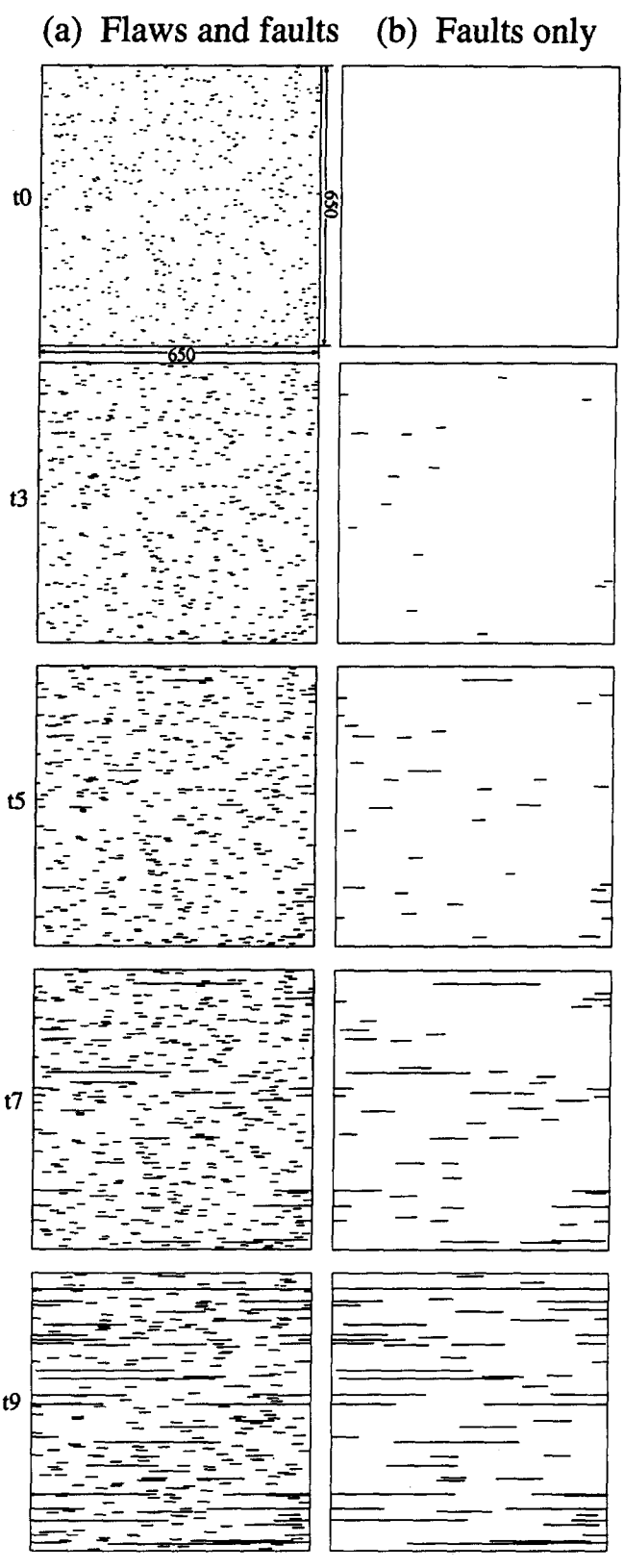

Fig. 4. (a) Synthetic fault maps created by the model after tx steps of model time. (b) Same maps as (a) except that flaws have been removed. A periodic boundary condition was used, so a fault that leaves the left edge connects to the same fault on the right.

the same recurrence interval. Initially, we ran models with small time steps, so that on average five faults experienced equivalent earthquakes for every increment of time. Those results were not significantly different from models run with large time steps, in which all faults experienced equivalent earthquakes for each increment of time. Therefore, for the models described below, a step of model time is equal to the recurrence interval of all of the faults in the population.

Figures 3, 4 and 5 graphically show the implementation of the linkage model. The following four steps summarize the computer model used to implement numerically the linkage model.

1. Random positions are assigned to 500 flaws of length $L_0 = 5$ parallel to the x-axis (a unimodal distribution). For each step of model time the following steps are performed.

2. For each flaw or fault tip, a search for other tips is performed. This is done in concentric circles with increasing radii until r_{max} (equation (15) and Fig. 3) is reached.

3. If a 'nearby' flaw or fault tip is found within the search circle, then linkage will occur as long as linkage creates a longer fault than would occur by fault growth (this criteria is implemented so that flaws and small faults do not slow the growth of large faults). The y-coordinate of the new fault is determined from the ratio of the lengths of the two old faults and their y-parallel separation (Fig. 3a). Alternatively, if a 'nearby' fault or flaw tip is not present, the flaw or fault grows by $\Delta L = \lambda L/2$.

4. Once this process is completed for both tips of all flaws and faults in the population, the fault length distribution is recorded. Steps 2 to 4 are iterated until the longest fault reaches the length of the model area.

The model generates a list of flaw and fault lengths at the end of each step of model time. We sort this list into descending length rank order, delete the flaws and plot

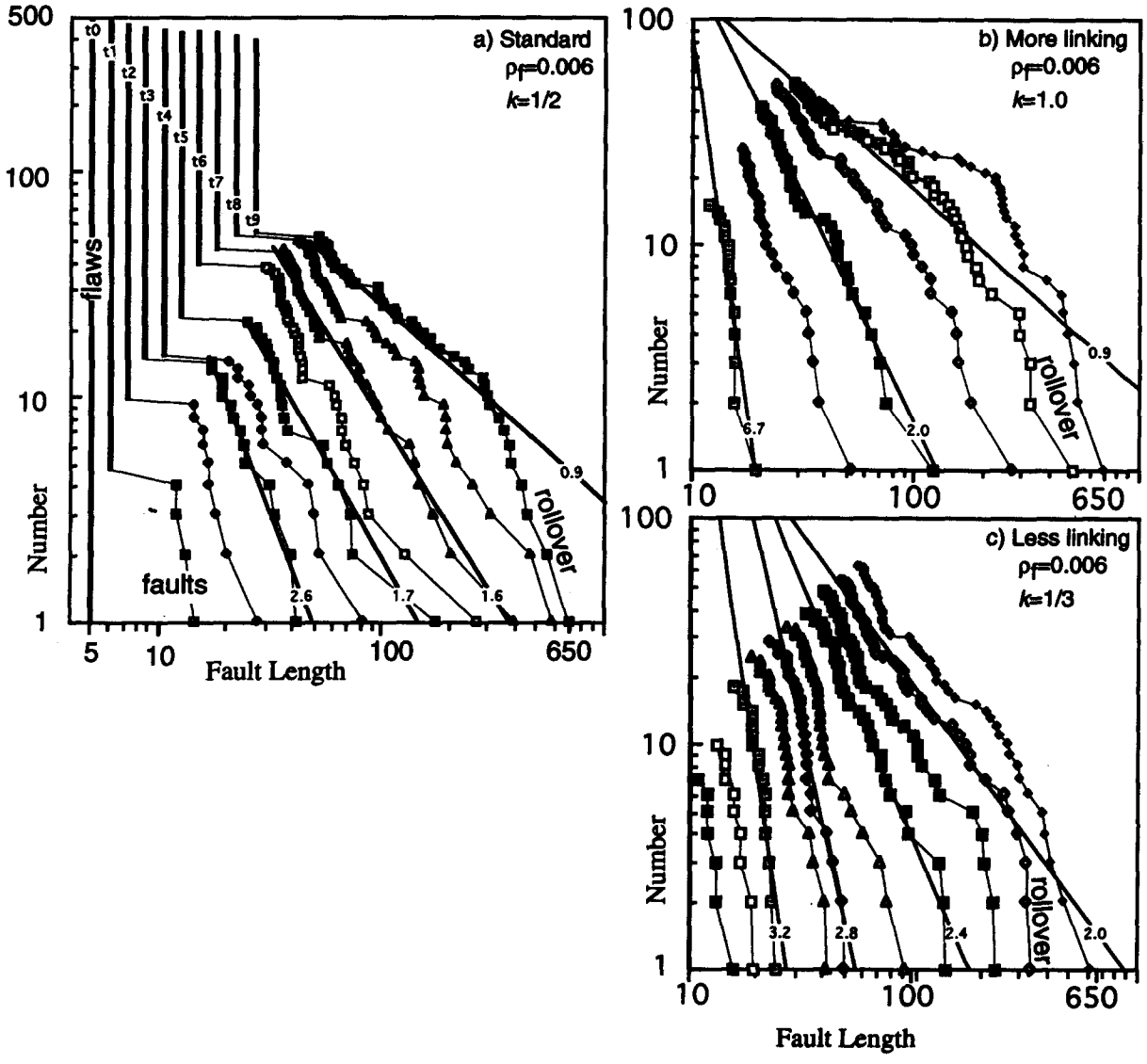

Fig. 5. Log–log plots of fault length data sets. (a) The top graph shows the results produced by the standard model with flaw distribution shown as vertical lines. (b) & (c) Model results of varying parameters from the standard model. The flaw population is not shown in these graphs. Notice the rollover which occurs on the last cycle on all data sets. In the model, the rollover occurs when the longest faults approach the length of the model region.

log number vs log fault length. A linear fit of the plot fixes the power-law exponent, C.

Linkage model results

A standard model with initial flaw density (ρ_f) set at 0.006 ($500 \times 5/650^2$), the search circle parameter (k) set to 0.5, and the fault growth model exponents of $E = 0$ and $F = 1$ was run four times. To investigate the effect of changing the first two parameters, the model was run twice, each with $\rho_f = 0.003$, $\rho_f = 0.012$, $k = 1$, $k = 0.33$, and $F = E = 1$. Flaw density was varied by reducing the number of initial flaws to 250 or using 325 units for the y dimension of the model area. The power-law exponent (C), linear correlation coefficient, number of faults, and the total fault length for all fourteen models were calculated and graphed as a function of model time in Fig. 6.

Do the synthetic fault populations fit a power-law length distribution? Yes. The three graphs in Fig. 5 show 25 fault populations, and 17 of those have linear correlation coefficients greater than or equal to 0.95. The fourth row of Fig. 6 shows the correlation coefficients for all fourteen model runs. The linear fit can be poor when the fault population set is small; however, once the population includes more than 30 faults, $R^2 \geq 0.95$ for 85% of the model results. In all the model runs, when the longest fault approaches the length of the model region, the long faults of the data sets define a steeper trend known as rollover (Fig. 5a). Like the rollover observed in the data presented in Fig. 1, the longest model faults were left out of the linear fit when rollover was observed.

How does the power-law exponent evolve? As shown in the third row of Fig. 6, C starts at high values (6.7–3) and decreases to between 2.4 and 0.9. In some cases, C increases slightly before decreasing. Importantly, C does not evolve to a constant value in the model. The decrease of C was ultimately limited when the length of the longest fault in the population reached the length of the model, and the model was stopped. There is no reason to believe that C would not continue to decrease if the model were larger.

If all is held constant, is there a random variation of the results? The standard model was run four times, and each of the other models run twice, so the importance of the initial random positions of the flaws can be assessed. When few (10–15) faults exist in the fault populations, the values of C can vary significantly between models with the same parameters; however, after more model time has passed and the fault populations contain more faults, the variation among like models is small (Fig. 6, row 3).

How do the synthetic results created by a growth model with $F = E = 1$ compare to the synthetic results with $F = 1$ and $E = 0$? The last column of Fig. 6 shows the results for $F = E = 1$. In contrast to the other model runs in which the recurrence interval is not a function of fault length ($E = 0$), in these two model runs the recurrence interval increased with fault length ($E = 1$). Qualitatively, the results are quite similar to the other twelve models; most importantly, C continuously decreased with model time. The final values of C are higher (steeper slopes) than for the other models, because the long fault growth was inhibited by long recurrence intervals.

How does altering the values of the parameters affect the outcome? The effects of changing the adjustable parameters are predictable and only affect the rates of fault growth (Figs. 5 and 6). Increased fault density ($\rho_f = 0.012$) or a larger search circle ($k = 1$) speeds the linkage process, causing C to decrease more rapidly. Decreased fault density ($\rho_f = 0.003$) or a smaller search circle ($k = 1/3$) slows the linkage process, causing C to decrease more slowly. Of course, model time is dimensionless; it is more instructive to normalize the model time axis by calculating the total fault strain for each model and then comparing the results. Strain is calculated by summing the geometric moments (Marrett & Allmendinger 1990, 1991) for the faults in the population, dividing by the deformed area to calculate total shear strain, and then recasting as natural strain (see Fig. 7 caption for more details). The 14 curves in Fig. 7 show a large variation of C at low strain, due entirely to random variation of the initial conditions, not the values of the adjustable parameters. At higher total strain ($\varepsilon > 0.01$), C varies between 0.9 and 1.6 for $F = 1$, $E = 0$ and between 1.8 and 2.4 for $F = E = 1$. Also notice that while the value of C may be showing asymptotic behavior, $C \rightarrow 0$ is more likely than $C \rightarrow 1$.

DISCUSSION OF THE FAULT LINKAGE MODEL

A simple geometric model incorporating fault growth and fault linkage produces a power-law distribution of fault lengths from a random spatial distribution of flaws. The model results also show a systematic decrease of the value of C (no equilibrium value of C was achieved). Next we compare the results from this model to actual fault length data (i.e. Fig. 1) and another model which simulates fault nucleation, linkage and growth (Cowie *et al.* 1993, 1995).

The linkage model produces a rollover (steeper trend) at long faults much like real data sets (compare Figs. 1 and 5). Marrett & Allmendinger (1992) attributed rollover of long faults to be due to sampling artifacts. Another interpretation is suggested by this model. Rollover in the model population occurs because the longest faults (those approaching the length of the model region) are unable to grow at rates sufficient to maintain the power-law distribution defined by the shorter faults. For example, to prevent rollover in Fig. 5(a), each of the eight longest faults would have had to more than double their length in the ninth growth cycle. This would be possible in a longer model region, but not when the

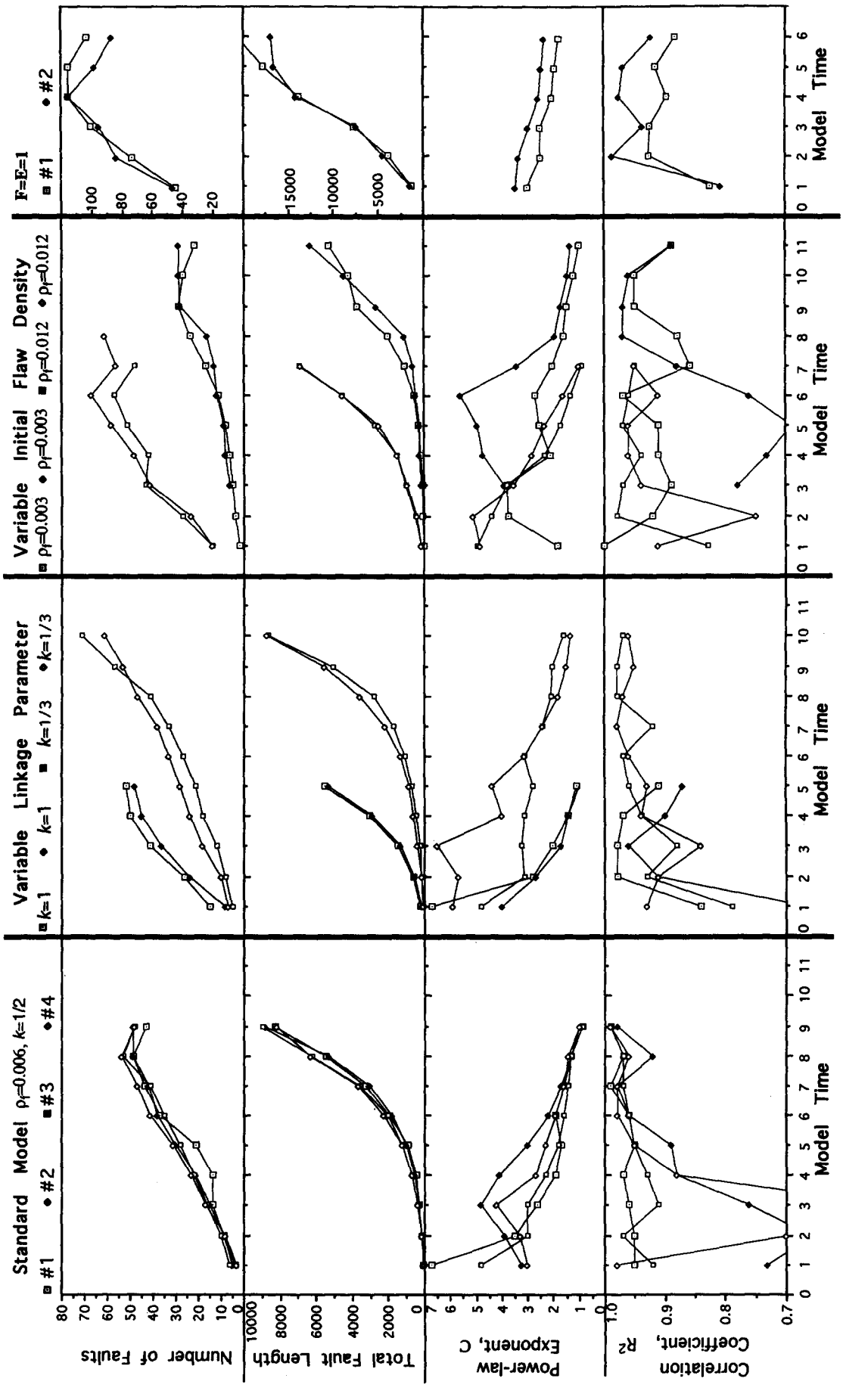

Fig. 6. Synthesis of results for sixteen runs of the fault growth and linkage model. The first column shows the results for the standard model. The second column shows the results when the linkage parameter is adjusted up ($k = 1$) and down ($k = 1/3$) from the standard model ($k = 1/2$). The third column shows the results when the initial flaw density is adjusted up ($\rho_f = 0.012$) and down ($\rho_f = 0.003$) from the standard model ($\rho_f = 0.006$) by changing the model size or number of initial flaws. The fourth column shows the results when growth exponents of $F = E = 1$ (Cowie & Scholz 1992c) were used instead of $F = 1$ and $E = 0$.

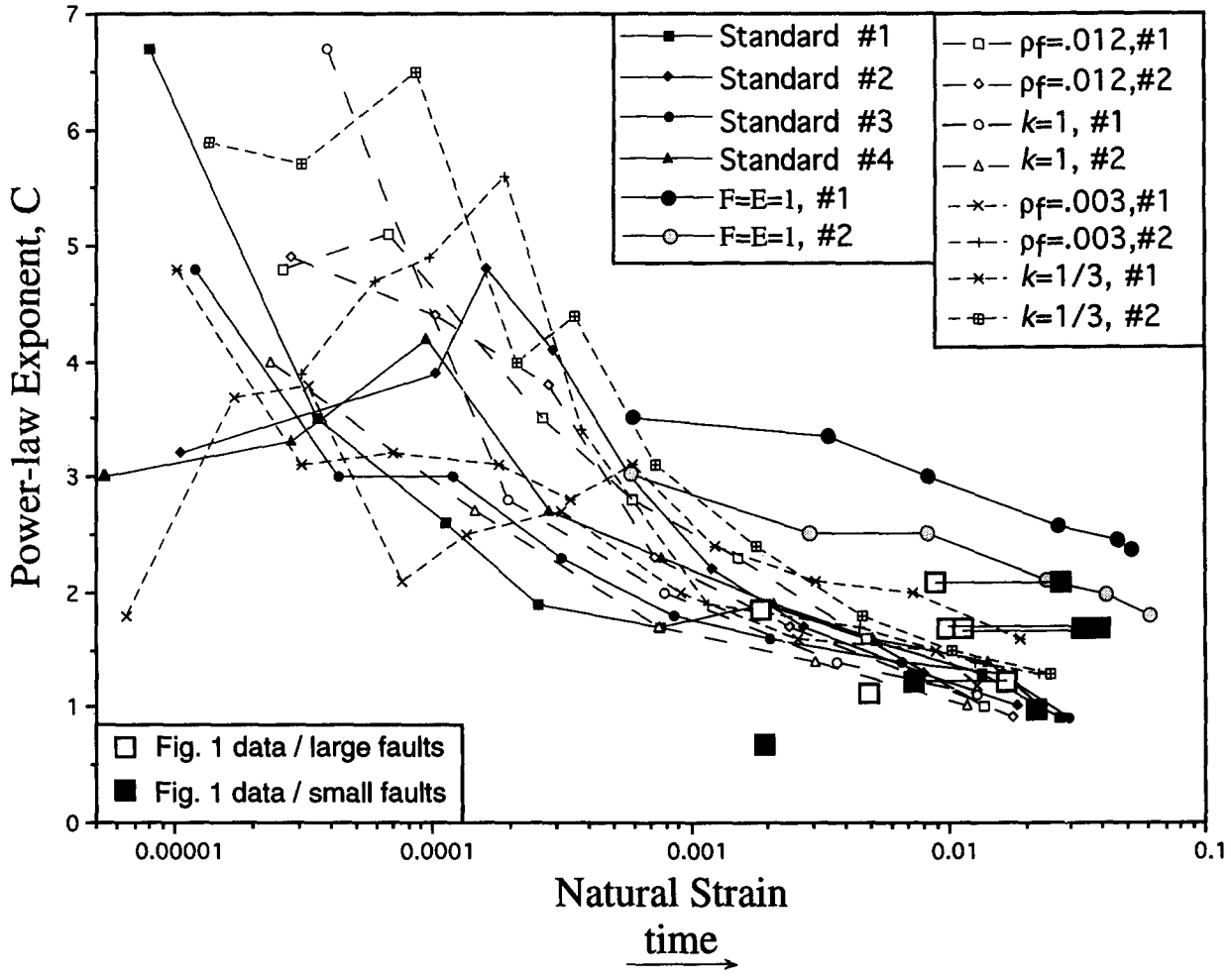

Fig. 7. Graph of power-law exponent versus natural strain due to faults. Strain was calculated by the method described in Marrett & Allmendinger (1990, 1991). A plate thickness of unity and a displacement relationship of $D = L/100$ were assumed (Scholz & Cowie 1990). This allows the geometric moment (M_g) of each model fault to be calculated from the fault length: $M_g = L^2/100$. The geometric moments for all faults were summed and the sum divided by the volume (650 × 650 × 1). This gives the total shear strain γ, which can easily be recast as natural strain, $\varepsilon = \ln(\gamma/2 + 1)$. Many more uncertainties are inherent in applying this procedure to natural fault populations. Most importantly, without knowing the orientations of faults, a tensor summation (Marrett & Allmendinger 1990) cannot be performed and the strain calculated must be considered a maximum. Other problems include choosing the thickness of the plate which the faults strain, and deciding whether the faults are large (faults that fully cut the plate) or small (faults that do not cut the plate). Despite these problems, strain was calculated for natural fault populations of Fig. 1, in order to directly compare that data to the model data. Except for two data sets (Chimney Rock and Yucca Mountain), natural strain was calculated using the large fault equation for geometric moment as was done with the synthetic data. The areas used for each data set are given in Fig. 1. The deformed volumes need not be calculated, as the plate thickness drops out of the equation for large faults. Except for two other data sets (Laramide and Basin-Range), the strain was also calculated using the small fault equation for geometric moment: $M_g = (\pi/4)\, L^3/100$. In this case the areas were multiplied by a thickness of 10 km to calculate volume. For data sets in which strain was calculated by both methods, a line connects the points of the same data set.

longest faults are already half the length of the model region. Since most faulted regions are finite in size because of stratigraphic or structural boundaries, perfect fault length data from most areas may show rollover on a log–log plot for the same reason as the model.

In all of the linkage models, the value of C decreased systematically with fault strain; there is no evidence that C approached a constant in the model runs (Figs. 6 and 7). Likewise, in the natural populations shown in Fig. 7, the relationship between C and fault strain is inconclusive; it is not possible to assess whether fault linkage is important at all stages of fault population evolution. For example, if it were observed that C reaches an equilibrium with respect to fault strain in natural populations, this could indicate that linkage ceases to be an important process of fault growth. Indeed, the fault linkage model maximizes the possibility of linkage, and especially favors linkage of longer faults because the faults are parallel. Because linkage depends critically upon the orientation of the faults, linkage in natural populations may not always be possible, and growth by tip propagation may dominate. In populations of non-parallel faults, linkage could be suppressed, leading to a stabilization or even increased value of C.

Figure 8 is a schematic diagram showing the processes governing the evolution of a model fault population through C-fault strain space. At any time, the evolution of the synthetic fault population depends on the balance

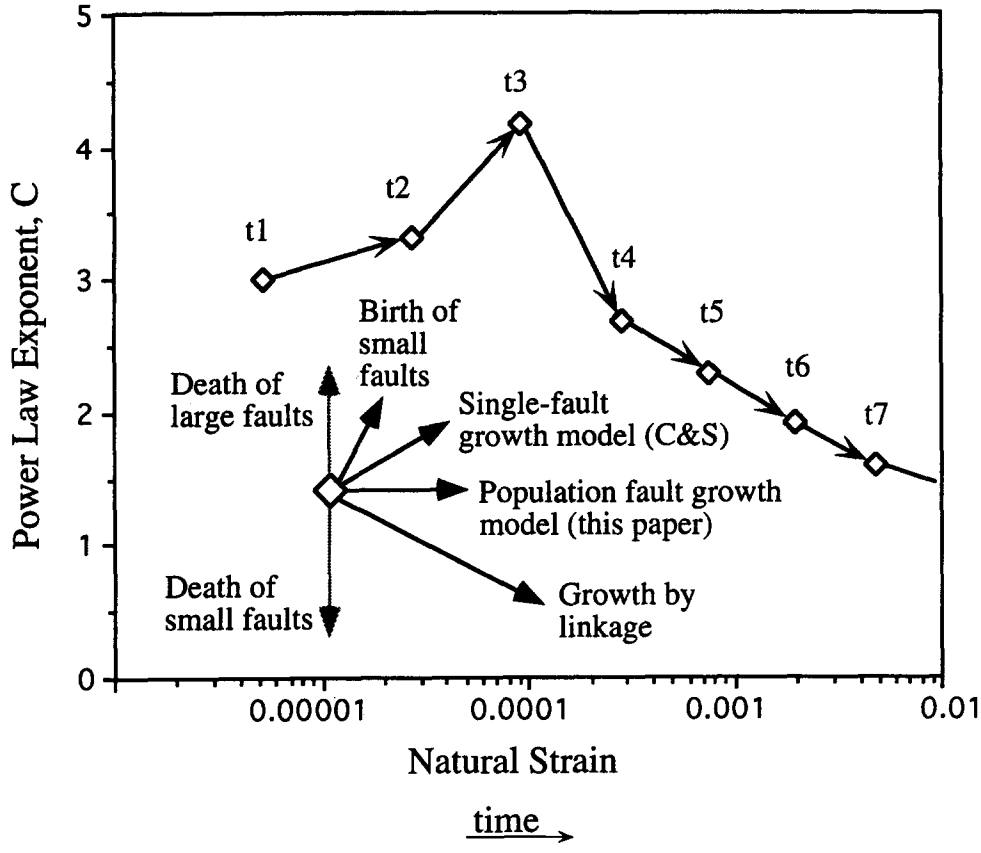

Fig. 8. Schematic diagram showing processes governing the evolution of a model fault population through C-fault strain space. As an example, the results from the model run Standard #4 are shown. See text for further explanation.

of three competing processes. Birth of new faults (by coalescence of flaws) increases the number of small faults without affecting the length of the long faults, increasing the value of C and simultaneously increasing the total strain. For the first two steps of model time, this process dominated in the example population shown. Fault growth by slip events was discussed in the first part of this paper. It was shown that in order to maintain a power-law distribution, a population fault growth model must also preserve the value of the power-law exponent. Thus, the population fault growth model plots as a horizontal line in Fig. 8. In contrast, the single-fault growth model ($F = E = 1$, Cowie & Scholz 1992c) causes C to increase with accumulated fault strain (Fig. 2); therefore, that model's vector in C-fault strain space points upward. The results of the fault linkage model (Figs. 6 and 7) show that linkage, which cannibalizes small faults to create larger faults, decreases the value of C while increasing total fault strain. In the example population shown, fault linkage dominated after the second step of model time, and C continuously decreased with total fault strain. The effect of two additional processes (birth of small faults and death of large faults) is also shown in Fig. 8, although this model simulated neither. In summary, for the population fault growth model ($F = E = 1$), Fig. 8 shows that as long as fault linkage occurs and is not balanced by birth of small faults or death of large faults, the value of C will systematically decrease with increased fault strain. Even with the single-fault growth model ($F = E = 1$), which causes C to increase, fault linkage dominated and the value of C decreased with fault strain (Fig. 7). If fault linkage and single-fault growth were carefully balanced, it might be possible to stabilize the value of C with respect to fault strain (a horizontal line on Fig. 8).

Cowie *et al.* (1993, 1995) develop and discuss a numerical rupture model which is used to simulate the nucleation and growth of faults in a plate. Their model starts with an 180 × 180 element lattice with a random spatial distribution of yield stress. When a constant velocity is applied along one edge of the lattice, fault nucleation, growth and linkage are simulated. The linkage model developed in this paper is strictly geometrical (nearness of fault tips), while the Cowie *et al.* (1993, 1995) model simulates anti-plane shear deformation of an elastic material. Despite the major differences in the model setup, the results produced by the two models are broadly similar. Both models produce a power-law distribution of fault lengths from a random spatial distribution of strength (flaws or yield stress elements). In both models, the values of C begins at a large value and decreases to less than 1.5 as fault strain increases. Cowie *et al.* (1995) argue that a constant value of C is eventually achieved when the deformation in the plate reaches saturation; in both models the decrease of C is limited by the small size of the model. Given much larger models, the value of C would probably continue decreasing in both cases.

CONCLUSIONS

A population fault growth model designed to insure a constant power-law distribution of fault lengths is significantly different to single-fault growth models, especially if constant moment release rate is required of the fault population. For the two types of models to converge, one or more of the assumptions of the population fault growth model must be rejected.

One possible solution to the dilemma is that fault linkage plays an important role in maintaining the power-law distribution. Indeed, it was found that linkage is a very effective process for creating a power-law length distribution from a population that initially does not have a power-law distribution. However, fault linkage does not cause the power-law exponent (C) to reach an equilibrium as fault strain increases.

More sophisticated models which attempt to balance the effects of various processes that affect a fault population's journey through C-fault strain space (Fig. 8) may be possible. It is also of critical importance to determine the relationship between C and fault strain in natural populations. Perhaps the power-law exponent's value and its evolution with increasing fault strain could reveal important information about the processes operative during fault growth.

Acknowledgements—We wish to thank Donald Turcotte and Richard Allmendinger for their ideas, criticism and support. The manuscript was improved due to reviews by J. Filbrandt, D. C. P. Peacock and especially P. Cowie. This work was financially supported by a Petroleum Research Foundation Grant to R. Allmendinger of Cornell University, where this work was the final chapter of the first author's doctoral thesis. R. Marrett acknowledges support from Amoco Production Research.

REFERENCES

Aki, K. 1981. A probabilistic synthesis of precursory phenomena. In: *Earthquake Prediction* (edited by Simpson, D. W. & Richards, P. G.). *Am. geophys. Un.* Maurice Ewing Vol. **4**, 556–574.

Blackstone, D. L., Jr. 1988. Traveler's guide to the geology of Wyoming. *Bull. Geol. Surv. Wy.* **67**.

Childs, C., Walsh, J. J. & Watterson, J. 1990. A method for estimation of the density of fault displacements below the limits of seismic resolution in reservoir formations. In: *North Sea Oil and Gas Reservoirs II* (edited by The Norwegian Institute of Technology). Graham & Trotman, London, 309–318.

Cladouhos, T. T. 1993. Quantitative Analysis of Faults: Fault Kinematics from the Andes of NW Argentina and SW Bolivia, a Finite Strain Method, and a Fault Growth Model. Ph.D. Dissertation, Cornell University, Ithaca, NY.

Cowie, P. A. & Scholz, C. H. 1992a. Physical explanation for displacement-length relationship of faults using a post-yield fracture mechanics model. *J. Struct. Geol.* **14**, 1133–1148.

Cowie, P. A. & Scholz, C. H. 1992b. Displacement-length scaling relationships for faults: data synthesis and discussion. *J. Struct. Geol.* **14**, 1149–1156.

Cowie, P. A. & Scholz, C. H. 1992c. Growth of faults by accumulation of seismic slip. *J. geophys. Res.* **97**, 11085–11095.

Cowie, P. A., Sornette, D. & Vanneste, C. 1993. Statistical physical model for the spatio-temporal evolution of faults. *J. geophys. Res.* **98**, 21809–21821.

Cowie, P. A., Sornette, D. & Vanneste, C. 1995. Multifractal scaling properties of a growing fault population. *Geophys. J. Int.* **122**, 457–469.

Dawers, N. H., Anders, M. H. & Scholz, C. H. 1993. Growth of normal faults: displacement–length scaling. *Geology* **21**, 1107–1110.

Davy, P. 1993. On the frequency–length distribution of the San Andreas fault system. *J. geophys Res* **98**, 12414–12151.

Dugdale, D. S. 1960. Yielding of steel sheets containing slits. *J. mech. phys. Solids* **8**, 100–104.

Gillespie, P. A., Walsh, J. J. & Watterson, J. 1992. Limitations of dimension and displacement data from single faults and the consequences for data analysis and interpretation. *J. Struct. Geol.* **14**, 1157–1172.

Griffith, A. A. 1920. The phenomenon of rupture and flow in solids. *Phil. Trans. Royal Soc. Lond.* **A221**, 163–198.

Griffith, A. A. 1924. The theory of rupture. In: *Proc. Int. Congr. Appl. Mech.* (edited by Biezeno, C. B. & Burgers, J. M.). Delft. Tech. Boeckhandel en Drukkerij J. Walter Jr.

Gudmundsson, A., 1987. Geometry, formation and development of tectonic fractures on the Reykjanes Peninsula, southwest Iceland. *Tectonophysics*, **139**, 295–308.

Gutenburg, B. & Richter, C. F. 1954. *Seismicity of the Earth and Associated Phenomena* (2nd edn). Princeton University Press, NJ.

Jamison, W. R. 1989. Fault-fracture strain in Wingate sandstone. *J. Struct. Geol.* **11**, 959–974.

Kakimi, T. 1980. Magnitude–frequency relation for displacement of minor faults and its significance in crustal deformation. *Bull. geol. Surv. Japan (Chishitsu Chosasho Geppo)* **31**, 467–487.

Kanamori, H. & Anderson, D. L. 1975. Theoretical basis of some empirical relations in seismology. *Bull. seism. Soc. Am.* **65**, 1073–1095.

Krantz, R. W. 1988. Multiple fault sets and three-dimensional strain: Theory and application. *J. Struct. Geol.* **10**, 225–237.

Main, I. G., Meredith, P. G., Sammonds, P. R. & Jones, C. 1990. Influence of fractal flaw distributions on rock deformation in the brittle field. In: *Deformation Mechanisms, Rheology and Tectonics* (edited by Knipe, R. J. & Rutter, E. H.). *Spec. Publ. geol. Soc. Lond.* **54**.

Marrett, R. A. & Allmendinger, R. W. 1990. Kinematic analysis of fault-slip data. *J. Struct. Geol.* **12**, 973–986.

Marrett, R. A. & Allmendinger, R. W. 1991. Estimates of strain due to brittle faulting: sampling of fault populations. *J. Struct. Geol.* **13**, 735–738.

Marrett, R. A. & Allmendinger, R. W. 1992. The amount of extension on 'small' faults: an example from the Viking Graben. *Geology* **20**, 47–50.

Martel, S. J. 1990. Formation of compound strike-slip fault zones, Mount Abbot quadrangle, California. *J. Struct. Geol.* **12**, 869–882.

Martel, S. J., Pollard, D. D. & Segall, P. 1988. Development of simple strike-slip fault zones, Mount Abbot quadrangle, Sierra Nevada, California. *Bull. geol. Soc. Am.* **100**, 1451–1465.

Peacock, D. C. P. 1991. Displacements and segment linkage in strike-slip fault zones. *J. Struct. Geol.* **13**, 1025–1035.

Peacock, D. C. P. & Sanderson, D. J. 1991. Displacements, segment linkage and relay ramps in normal fault zones. *J. Struct. Geol.* **13**, 721–733.

Pollard, D. D. & Segall, P. 1987. Theoretical displacements and stresses near fractures in rock: With applications to faults, joints, veins, dikes, and solution surfaces. In: *Fracture Mechanics of Rock* (edited by Atkinson, B. K.). Academic Press, London.

Scholz, C. H. & Cowie, P. A. 1990. Determination of total strain from faulting using slip measurements. *Nature* **346**, 837–839.

Scholz, C. H., Dawers, N. H., Yu, J.-J., Anders, M. H. & Cowie, P. A. 1993. Fault growth and fault scaling laws: preliminary results. *J. geophys. Res.* **98**, 21951–29161.

Scott, R. B. & Castellanos, M. 1984. Stratigraphic and structural relations of volcanic rocks in drill holes USW GU-3 and USW G-3, Yucca Mountain, Nye County, Nevada. *U.S. Geol. Surv. Open-file Rep.* **84-491**.

Segall, P. & Pollard, D. D. 1980. Mechanics of discontinuous faults. *J. geophys. Res.* **85**, 4337–4350.

Segall, P. & Pollard, D. D. 1983. Nucleation and growth of strike-slip faults in granite. *J. geophys. Res.* **88**, 555–568.

Shaw, H. R. & Gartner, A. E. 1986. On the graphical interpretation of paleoseismic data. *U.S. Open-File Rep* **86-394**.

Stewart, J. H. 1980. Geology of Nevada. *Spec. Pub. Nev. Bur. Mines & Geol.*

Suppe, J. 1985. *Principles of Structural Geology*. Prentice-Hall, Inc., NJ.

Tapponier, P. & Brace, W. F. 1976. Development of stress-induced microcracks in Westerly granite. *Int. J. Rock Mech. Min. Sci.* **13**, 103–112.

Turcotte, D. L. 1992. *Fractals and Chaos in Geology and Geophysics*. Cambridge University Press, Cambridge.

Walsh, J. J. & Watterson, J. 1987. Distributions of cumulative dis-

placement and seismic slip on a single normal fault surface. *J. Struct. Geol.* **9**, 1039–1046.

Walsh, J. J. & Watterson, J. 1988. Analysis of the relationship between displacements and dimensions of faults. *J. Struct. Geol.* **10**, 239–247.

Walsh, J. J. & Watterson, J. 1992. Populations of faults and fault displacements and their effects on estimates of fault-related regional extension. *J. Struct. Geol.* **14**, 701–712.

Villemin, T. & Sunwoo, C. 1987. Distribution logarithmique self-similaire des rejets et longueurs de failles: example du Bassin Houiller Lorrain. *C. r. Acad. Sci., Paris* **305**, 1309–1312.

Wong, T.-F., Fredrich, J. T. & Gwanmesia, G. D. 1989. Crack aperture statistics and pore space fractal geometry of Westerly granite and Rutland quartzite: implications for an elastic contact model of rock compressibility. *J. geophys. Res.* **94**, 10267–10278.